Eddy Advective and Diffusive Transports of Heat and Salt in the Southern Ocean

MEI-MAN LEE, A. J. GEORGE NURSER, A. C. COWARD, AND B. A. DE CUEVAS

James Rennell Division for Ocean Circulation and Climate, National Oceanography Centre, Southampton, Southampton, United Kingdom

(Manuscript received 28 February 2006, in final form 28 June 2006)

ABSTRACT

There are two distinct mechanisms by which eddies provide systematic transport of tracer on isopycnals: the advective transport, associated with the slumping of isopycnals, and the diffusive transport, associated with down-gradient diffusion. Depending on the large-scale tracer distribution, eddy advective transport has either the same direction as or opposite direction to eddy diffusive transport. As a consequence, eddy advection and eddy diffusion can reinforce each other for some tracers but oppose each other for other tracers. Using scaling analysis, it is argued that the relative directions of eddy advective and diffusive transports can be determined simply from the relative slopes of tracers and isopycnals. An eddy-resolving (1/12°) global ocean model is used to illustrate the two eddy transport mechanisms for temperature and salinity in the Southern Ocean. Applications to other tracers, such as oxygen, are discussed. The diagnosed eddy diffusivity for temperature (and salinity) is found to be considerably different from the eddy diffusivity for eddy advective transport velocity.

1. Introduction

The transport of properties by baroclinic eddies in the ocean has been widely regarded as potentially important for the time-mean budget of properties. However, eddy transports in the ocean are poorly observed quantities. Based on the large-scale heat budget, it is thought that eddy heat transport in the Southern Ocean is of first-order importance relative to the total heat transport (Nowlin and Klinck 1986; Gorden and Owens 1987). Studies from the quasi-global compilation of current-meter data (Wunsch 1999) and the synthesis of altimeteric data (Stammer 1998) show that in the Southern Ocean the magnitude of eddy heat transport is modest, but the zonally integrated transport probably dominates the southern high-latitude heat budget. In contrast, the importance of eddy salt transport for the salt budget is unclear. An altimeter-derived eddy salt transport (Stammer 1998) suggests that the implied eddy freshwater transport rarely exceeds 0.05 Sv (1 Sv $\equiv 10^6$ m^3 s^{-1}) over the Southern Ocean, and so is not important for the total freshwater transport (Wijffels 2001). The question is why eddy transport is less important for the salt budget than it is for the heat budget.

For modeling climate change, it is crucial that eddy transport and eddy-mean flow interaction are properly represented. There are two distinct mechanisms by which eddies transport properties on isopycnals: the advective transport, associated with an eddy transport velocity resulting from baroclinic instability, and the diffusive transport, associated with down gradient diffusion. Gent and McWilliams (1990, hereinafter GM90) proposed an eddy parameterization to represent eddy-induced advective velocity along isopycnals. Griffies (1998) combined eddy isopycnic diffusion with the GM90 parameterized eddy advection into one diffusive tensor. These subgrid-scale parameterizations have significantly improved climate models (Danabasoglu et al. 1994; Hirst et al. 2000).

The transport of tracers by eddy advection is not necessarily in the same direction as that by eddy diffusion. For instance, Lee and Williams (2000) showed that whether eddy advective and diffusive transport enhance or oppose each other depends on the lifetime of the tracer and the location of the tracer source. Their idealized experiments suggested that for the nutrient transport in the Southern Ocean, eddy advection and

Corresponding author address: Dr. Mei-Man Lee, James Rennell Division for Ocean Circulation and Climate, National Oceanography Centre, Southampton, Empress Dock, Southampton SO14 3ZH, United Kingdom.
E-mail: mmlee@noc.soton.ac.uk

DOI: 10.1175/JPO3057.1

diffusion are likely to oppose each other over the euphotic zone but reinforce each other at depth.

In this study, we explore eddy advective and diffusive transports of temperature and salinity. The aim is to differentiate the effect of eddy advection from eddy diffusion on the transport of heat and salt. By doing so, we find that we can explain why eddy salt transport is relatively less important for the salt budget.

Section 2 explains the basic idea of how the eddy transport of tracer resulting from advection and diffusion can behave differently according to the large-scale tracer distribution. Sections 3 and 4 gives the model details and the time-mean states of the model. In section 5, model eddy transports are diagnosed. In section 6, the basic idea is generalized so that the relative directions of eddy advective and diffusive transports are determined from the relative slopes of the tracer and isopycnal. In section 7, eddy diffusivities are diagnosed. Section 8 is the conclusions.

2. Eddy advective and diffusive transport

When analyzing data from observations or from global eddy-resolving models, it is traditional to take, say, $v'T'$ for the eddy heat flux. Although it is possible to project $v'T'$ into along- and across-isopycnic components in the interior, there are problems near the boundaries where isopycnals outcrop (Held and Schneider 1999; Nurser and Lee 2004b). Here, we will use an isopycnic framework from which eddy transport along isopycnals can be uniquely defined.

The evolution of tracer substance in an isopycnic layer is governed by

$$\frac{\partial}{\partial t}(\tau h) + \nabla \cdot (\mathbf{u}\tau h) = \mathcal{H}, \tag{1}$$

where τ is the tracer concentration, h is the isopycnic layer thickness (thus, τh is the tracer substance per unit area), $\mathbf{u} = (u, v)$ is the velocity along isopycnal (assuming no diapycnic flow), ∇ is the horizontal gradient, and $\mathcal{H}$ is the source/sink for the tracer substance. If τ is temperature, then τh is thought of as heat content and $\mathcal{H}$ as heating/cooling.

The time mean of total transport can be separated into advection and diffusion,

$$\overline{\mathbf{u}\tau h} = \hat{\mathbf{u}}\hat{\tau}\overline{h} + \widehat{\mathbf{u}''\tau''}\overline{h}, \tag{2}$$

where the overbar is the time average along the isopycnal, the caret is the layer thickness–weighted time average, for example, $\hat{\varphi} = \overline{\varphi h}/\overline{h}$, and the double prime is the deviation from the caret quantity, for example, $\varphi'' = \varphi - \hat{\varphi}$.

The derivation of (2) is straightforward (e.g., Dukowicz and Greatbatch 1999; McDougall and McIntosh 2001). The first term on the rhs of (2) is the total advective transport by the transport velocity $\hat{\mathbf{u}}$. The second term represents the eddy diffusion of tracer concentration, which is usually parameterized as $\widehat{\mathbf{u}''\tau''} = -\mathbf{K} \cdot \nabla\hat{\tau}$, where $\mathbf{K}$ is the eddy diffusion tensor.

Following McDougall and McIntosh (2001), the transport velocity $\hat{\mathbf{u}}$ is further separated into the Eulerian time-mean velocity and the eddy-induced velocity,

$$\hat{\mathbf{u}} = \overline{\mathbf{u}}_{\text{eu}} + \overline{\mathbf{u}}_{\text{eddy}}, \tag{3}$$

where $\overline{\mathbf{u}}_{\text{eu}}$ is time-averaged velocity on constant z, and then is remapped onto isopycnic layers. A more precise definition is given in section 4b.

From (2) and (3), we have

$$\overline{\mathbf{u}\tau h} = \overline{\mathbf{u}}_{\text{eu}}\hat{\tau}\overline{h} + \overline{\mathbf{u}}_{\text{eddy}}\hat{\tau}\overline{h} + \widehat{\mathbf{u}''\tau''}\overline{h}. \tag{4}$$

The total transport of substance in an isopycnal layer consists of the transport by time-mean Eulerian flow (first term), the transport by eddy advection (second term), and eddy diffusion (third term). The separation of eddy advective transport from eddy diffusive transport highlights that eddy transport of a substance is driven by two fundamentally different processes. The eddy advective transport depends on the transport velocity, which is approximately the correlation between the eddy velocity and isopycnic layer thickness, whereas the diffusive transport is the correlation between the eddy velocity and tracer on an isopycnal.

Thus, the budget for any tracer substance in an isopycnic layer is

$$\frac{\partial}{\partial t}(\hat{\tau}\overline{h}) + \nabla \cdot (\overline{\mathbf{u}}_{\text{eu}}\hat{\tau}\overline{h}) + \nabla \cdot (\overline{\mathbf{u}}_{\text{eddy}}\hat{\tau}\overline{h}) + \nabla \cdot (\widehat{\mathbf{u}''\tau''}\overline{h}) = \overline{\mathcal{H}}. \tag{5}$$

The distribution of the time-averaged tracer substance $\hat{\tau}\overline{h} = \overline{\tau h}$ is controlled through the Eulerian mean advection, the eddy advection, the eddy diffusion, and the source/sink.

Directions of advective and diffusive transports

In the following, we discuss the *direction* of zonally and vertically integrated eddy transport. For simplicity, we consider the meridional eddy transport of tracer in a zonal channel,

$$\overline{v}_{\text{eddy}}\hat{\tau}\overline{h} - \kappa\frac{\partial\hat{\tau}}{\partial y}\overline{h}, \tag{6}$$

where eddy diffusion is parameterized with eddy diffusivity κ.

We will use scale analysis for a two-layer fluid. Assume that layer thickness is H for each layer, and the eddy velocity is V in the upper layer and $-V$ in the lower layer. The vertically integrated advective transport is scaled as

$$V(\tau_u - \tau_l)H, \tag{7}$$

and the vertically integrated diffusive transport is scaled as

$$-\frac{1}{L}\kappa(\tau_n - \tau_s)H, \tag{8}$$

where $\tau_{u,l}$ is the tracer in the upper and lower layer, respectively, $\tau_{n,s}$ is the vertically averaged tracer at the north and south, respectively, and L is the length scale over which the meridional gradient of tracer is taken.

Thus, the direction of diffusive transport is always down the mean meridional tracer gradient on isopycnals, whereas the direction of advective transport depends on the isopycnic eddy velocity and the mean vertical tracer gradient. Thus, depending on the eddy transport velocity and spatial distribution of tracer, the advective and diffusive transports can have the same or opposite sign.

The directions of eddy advective and diffusive transports for temperature and salinity are illustrated using the schematic in Fig. 1. The eddy transport velocity is assumed to be poleward in the upper layer and equatorward in the lower layer. The upper layer is warmer than the lower layer and so the net eddy heat transport is poleward (indicated by the straight-shaded arrow). However, if the upper layer is fresher than the lower layer, then the eddy advective salt transport would be equatorward. Thus, the eddy advective transport of tracer depends on the vertical gradient of tracers. On the other hand, because water is cooler toward the pole and warmer toward the equator, down-gradient diffusion leads to poleward diffusive heat transport (indicated by the curved, shaded arrows). Similarly, if the water is fresher toward the pole and saltier toward the equator, then eddy diffusive salt transport is also poleward.

Because the vertical and meridional gradients of temperature differ from those of salinity, eddy advection and diffusion together can have different net effects on heat and salt transports. If temperature and salinity distributions are as in the schematic in Fig. 1, then eddy advection and eddy diffusion enhance each other for heat transport but oppose each other for salt transport. In the following, this idea is verified using an eddy-resolving global ocean model.

3. Model

We diagnose a 1/12° global ocean model, the Ocean Circulation and Climate Advanced Model (OCCAM). The model setup and forcing is similar, apart from horizontal resolution, to that of the 1/4° model described in Coward and de Cuevas (2005). The physical framework is based on the Modular Ocean Model (MOM) (Pacanowski 1995) and incorporates several important developments (Webb et al. 1998). The latest version includes a mixed layer, sea ice, and a variable bottom box. The vertical resolution is 66 levels with level thickness varying from 5 m at the surface to 200 m at depth. The topography was derived from a 2-min gridded latitude–longitude composite global bathymetric dataset, based on the Sandwell and Smith (1995) topography joined to Jakobsson et al.'s (2000) Arctic Ocean bathymetry north of 72°N and to the 5-min Digital Bathymetric Data Base (DBDB5) south of 72°S. Median values for each 1/12° grid cell were used. The topography was not smoothed, but certain straits were deepened and the ocean depth was constrained to be everywhere at least two grid boxes (~11 m) deep.

There is no explicit horizontal diffusion of tracers, although the advection scheme has implicit biharmonic diffusion. There is an explicit vertical diffusion with diffusivity 0.5 $cm^2\ s^{-1}$. For momentum, the eddy viscosity is 1 $cm^2\ s^{-1}$ in the vertical direction and 50 $m^2\ s^{-1}$ in the horizontal plane.

The model is Boussinesq and so is volume conserving rather than mass conserving. It includes a nonlinear free surface, in which the thickness of the topmost box responds to freshwater inputs such as precipitation and evaporation. Salinity changes solely as a consequence of dilution, and so the total globally integrated salt mass remains constant.

The surface fluxes are as in Coward and de Cuevas (2005). They were supplied by the National Center for Atmospheric Research (NCAR), adjusted according to Large et al. (1997) and Large and Nurser (2001, henceforth LN01). Evaporation, together with latent, sensible, and long-wave heat fluxes, is calculated at each time step from bulk formulas, using interpolated 6-hourly atmospheric fields (with reduced humidity; see LN01) from the National Centers for Environmental Prediction (NCEP) reanalysis (Kalnay et al. 1996) and model sea surface temperature. Monthly averaged insolation is derived from the International Satellite Cloud Climatology Project (ISCCP) daily data (Bishop

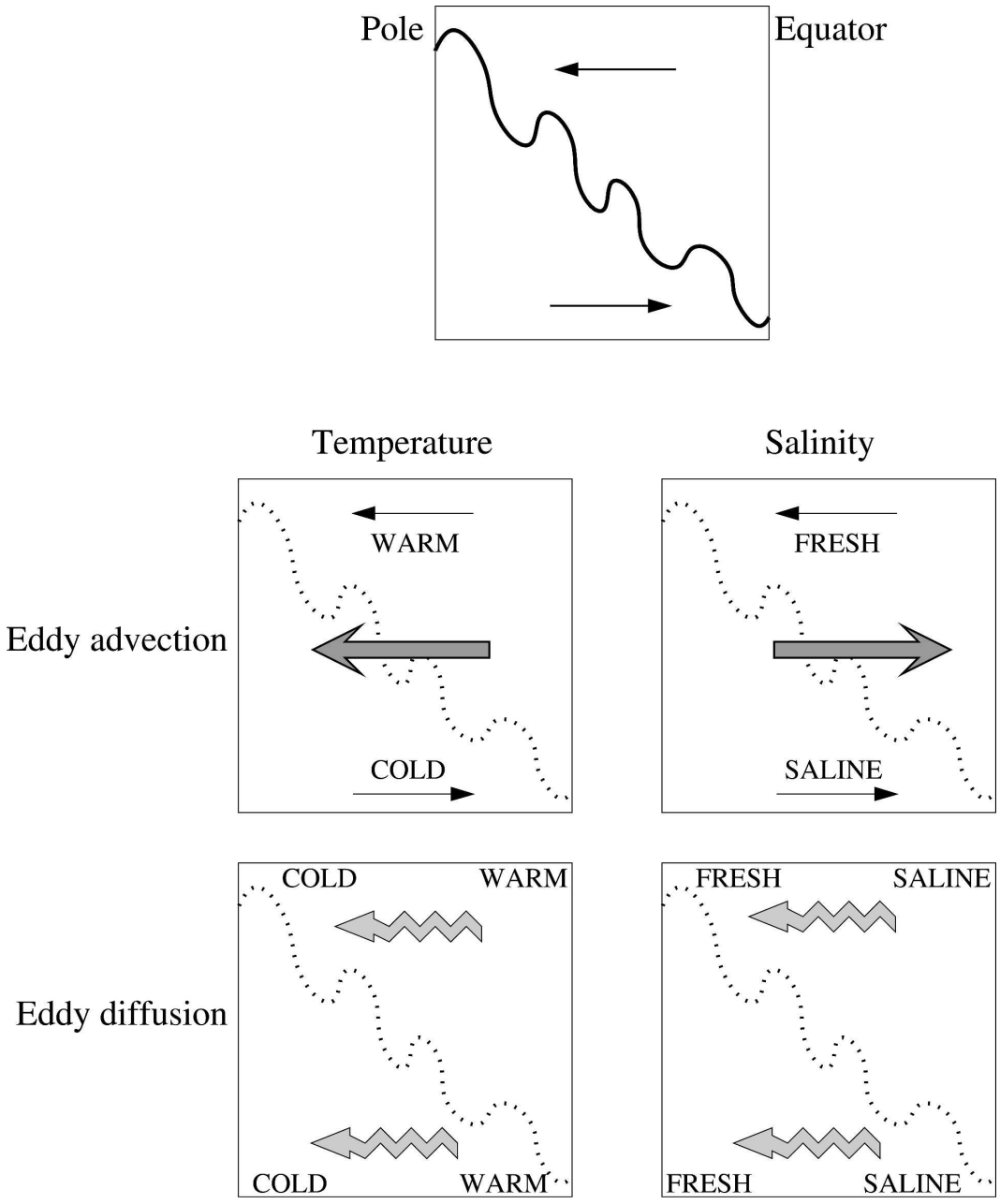

FIG. 1. Schematic illustrating that for (top) a given eddy transport velocity, (middle) the direction of eddy advective transport (straight shaded arrows) is determined by the across-isopycnal vertical gradient of tracer, and (bottom) the direction of eddy diffusive transport (curved shaded arrows) is determined by the along-isopycnal meridional gradient of tracer. Thus, advective transport and diffusive transport enhance each other for temperature but oppose each other for salinity.

et al. 1997) where possible, and otherwise from the ISCCP climatological values. It is then reduced by a factor of 0.875 (LN01). A constant oceanic albedo of 7% is further assumed.

In its default mode, the model linearly interpolates in time between monthly mean values of insolation to provide values at each time step. However, the model runs diagnosed here include a diurnal cycle. The insolation throughout each (UTC) day is supposed proportional to the sine of the sun's elevation above the horizon. The constant multiplying the sine is calculated at the beginning of each day, for each point, so as to ensure that the total insolation over the following day is the same as that given by the default scheme.

Precipitation is a blend of microwave climatological values (Spencer 1993) and merged observations (Xie and Arkin 1996). There is no explicit runoff field. Instead, freshwater input is applied so as to relax surface salinity back to monthly climatological values from the *World Ocean Atlas* (Boyer et al. 1998) with a piston velocity such that the upper 20 m would relax back to the climatological values on a time scale of 30 days. An additional globally uniform freshwater input is applied to prevent large variations in the total ocean volume. This freshwater input is calculated so as to return the globally averaged ocean height back to zero, with a relaxation time of 30 days. The surface forcing over sea ice is discussed in Aksenov (2002). The model is integrated from rest with initial tracer fields from the annual mean World Ocean Circulation Experiment Special Analysis Center climatological values (Gouretski and Jancke 1996).

The model has so far been run for the 1985–95 period. Data are averaged online at 5-day intervals. In this study, we analyze model data for the 1988–92 period and focus on the Southern Ocean south of 30°S. The z-level data are binned into 80 fixed but unevenly spaced potential density layers (referenced to 1940 m: σ_2).[1] The density classes are given in the appendix. We use a binning procedure such that the properties (mass, heat, salt) and their transports are conserved. For each model grid cell, if the potential density σ_2 lies between the predetermined density classes, $\sigma_{2,k} < \sigma_2 \le \sigma_{2,k+1}$, then we define a fraction $\chi = (\sigma_{2,k} - \sigma_2)/(\sigma_{2,k+1} - \sigma_{2,k})$. The grid cell thickness dz is partitioned into χdz for the $\sigma_{2,k}$ layer and $(1 - \chi)dz$ for the $\sigma_{2,k+1}$ layer. The transport vdz is binned in a similar way, as are heat and salt and their transports, that is, Tdz, Sdz, $vTdz$, and $vSdz$.

4. Time-mean states

The mean fields described below are 5-yr averages after the initial 3-yr spinup. Given the short run of the model, the water mass distribution is still close to the initial state. However, we think this should not affect eddy transport qualitatively, which is the main objective of the paper. Here, we only discuss the mean quantities that are relevant to this study. Other mean quantities will be reported in a separate study where comparison with lower-resolution model runs will be carried out.

All figures shown in this paper are zonally integrated quantities. For a given quantity ϕ, we denote $\{\phi|_z\}$ for zonal averaging on constant height, $[\phi]$ for zonal averaging on isopycnals without any weightings, and $\langle\phi\rangle$ for zonal averaging on isopycnals weighted by the time-mean layer thickness, $\langle\phi\rangle = [\phi\overline{h}]/[\overline{h}]$. Thus, $\langle\hat{T}\rangle = [\hat{T}\overline{h}]/[\overline{h}] = [\overline{T}\overline{h}]/[\overline{h}]$ represents isopycnic averaging weighted by layer thickness both zonally and temporally. For visualization, isopycnically averaged quantities are also remapped onto depth coordinates using the temporal and zonal mean height of isopycnals $[\tilde{z}]$ (Nurser and Lee 2004a). We will use the same notations for remapped quantities as for the isopycnically averaged quantities.

a. Temperature and salinity

The isopycnic mean temperature $\langle\hat{T}\rangle$ and Eulerian mean temperature $\{\overline{T}|_z\}$ are shown in Fig. 2. The isopycnic layer thickness–weighted averaging preserves the characteristics of temperature better than the Eulerian averaging because different water masses are mixed when averaged at a constant height. At a given latitude, isopycnic mean temperature at the surface is the mean temperature of the lightest water that ever occurs at that latitude, whereas Eulerian mean temperature at the surface is the average surface temperature at that latitude. Thus, if the salinity effect is small, then isopycnic mean temperature is warmer than Eulerian mean temperature at the surface but cooler at depth (Fig. 2c). At 50°S, the isopycnic mean temperature is warmer than the Eulerian mean temperature by at least 2°C for the top 150 m and cooler by 1°C at 800 m and by 0.6°C near the bottom. Near the Antarctic at 76°S, very cold water with −1.6°C temperature is found along the slope from the shelf to the bottom. In contrast, the signature of cold water along the slope is absent from the Eulerian averaging.

Similar contrast between isopycnic and Eulerian averaging is also seen in the salinity field (Fig. 3). The isopycnic mean salinity $\langle\hat{S}\rangle$ shows the fresh Antarctic Intermediate Water (AAIW) with a salinity minimum of $S < 34.4$ at 1100 m near 50°S. The AAIW layer maintains a thickness about 250 m at 30°S. In contrast, the Eulerian mean salinity $\{\overline{S}|_z\}$ has a less pronounced AAIW. Near the Antarctic, isopycnic averaging gives fresher surface waters than the Eulerian averaging. The difference between the isopycnic average and Eulerian average can be up 0.15 psu for the AAIW and 0.4 psu for the surface waters (Fig. 3c). Below 2000 m, the Lower Circumpolar Deep Water (LCDW) characterized by the high salinity $S > 34.7$ enters at 30°S below 2000 m and ascends to 700 m at 65°S. There is not much difference between the two averages at these depths except at the slope near the Antarctic.

[1] We are aware that it is not entirely satisfactory to use σ_2 near the surface and that some of the near-surface features in our analysis might be affected.

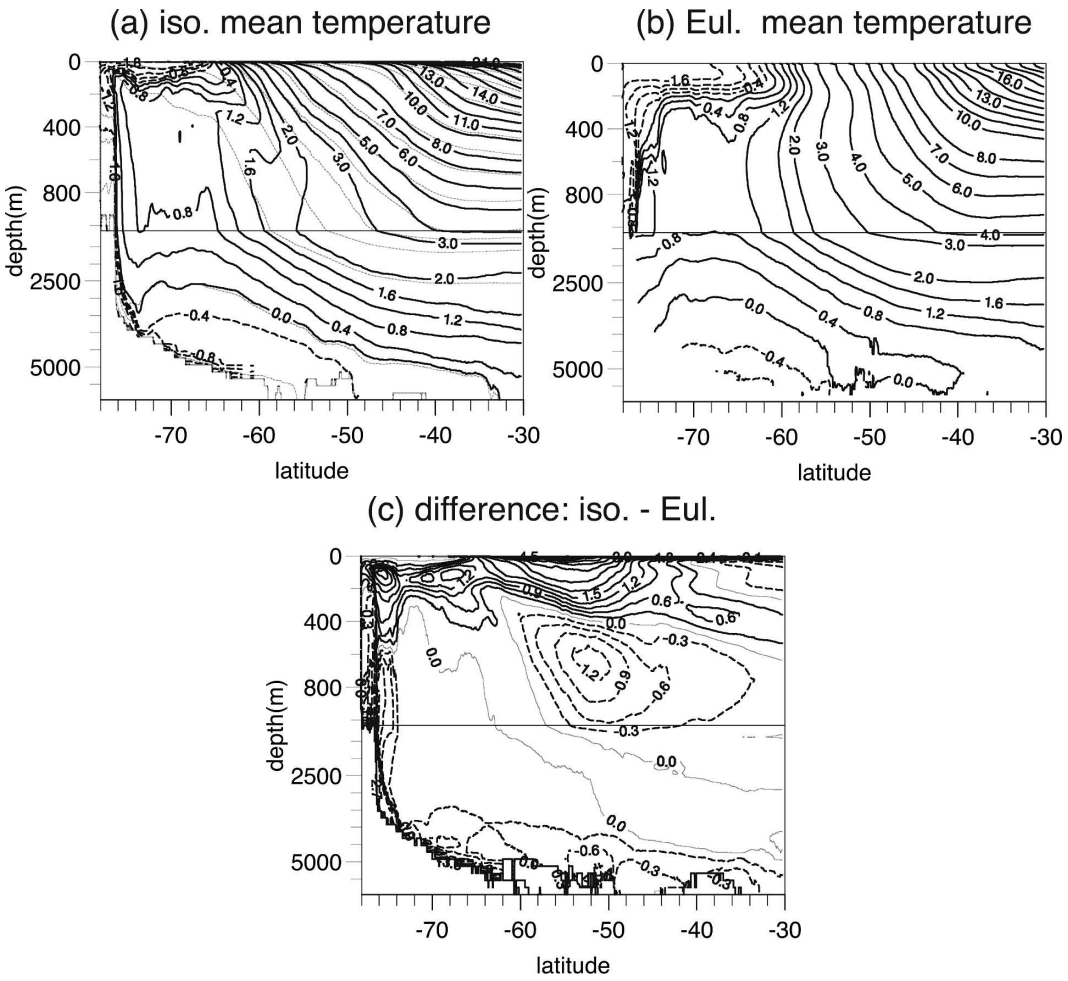

FIG. 2. The time and zonal mean temperature (a) isopycnic layer thickness–weighted mean temperature $\langle \hat{T} \rangle$ remapped to z using the mean height of isopycnals, (b) Eulerian-mean temperature $\{\overline{T}|_z\}$, averaged on z, and (c) the difference between (a) and (b). The contour interval in (a) and (b) is 1°C interval for temperature above 2° and 0.4°C interval for temperature below 2°C. The contour interval in (c) is 0.3°C. The top 1100 m are expanded for visualization. The thin dashed lines superimposed in (a) show the mean depth of isopycnals $[\bar{z}]$, where the density values are as labeled in Fig. 5c, below.

b. Transport streamfunction

1) TOTAL

Figure 4 shows the 5-yr average of the zonally integrated total meridional transport streamfunction in σ_2 coordinates,

$$\psi(y, \rho) = \int \int_{\rho}^{\rho_{\max}} \overline{vh}\, d\rho\, dx.$$

Superimposed on the streamfunction in Fig. 4 are the surface heat, freshwater, and buoyancy flux binned into σ_2 density classes. The streamfunction is also remapped onto depth coordinates and is shown in Fig. 5a.

The usual three overturning cells are present: a subtropical cell in the lighter density classes ($\sigma_2 < 35.5$), a subpolar cell in the intermediate density classes ($35.5 < \sigma_2 < 36.76$), and a deep cell. The subtropical cell is about 16 Sv at 30°S, which is comparable to 19 Sv in the Fine-Resolution Advanced Model (FRAM) (Döös and Webb 1994) and 14 Sv in earlier version of the OCCAM (Lee and Coward 2003). The lighter surface flow moves poleward and becomes denser by evaporation and some cooling to form 12°–14°C water, which may be identified as mode water. The equatorward flow returns at depths of about 200–400 m and stays at more or less the same density presumably as a result of mixing compensating surface cooling and evaporation.

In the intermediate density classes, there is a clockwise subpolar cell about 8 Sv with the Upper Circumpolar Deep Water (UCDW) flowing poleward at 1000–2000 m, and then becoming lighter by surface heating

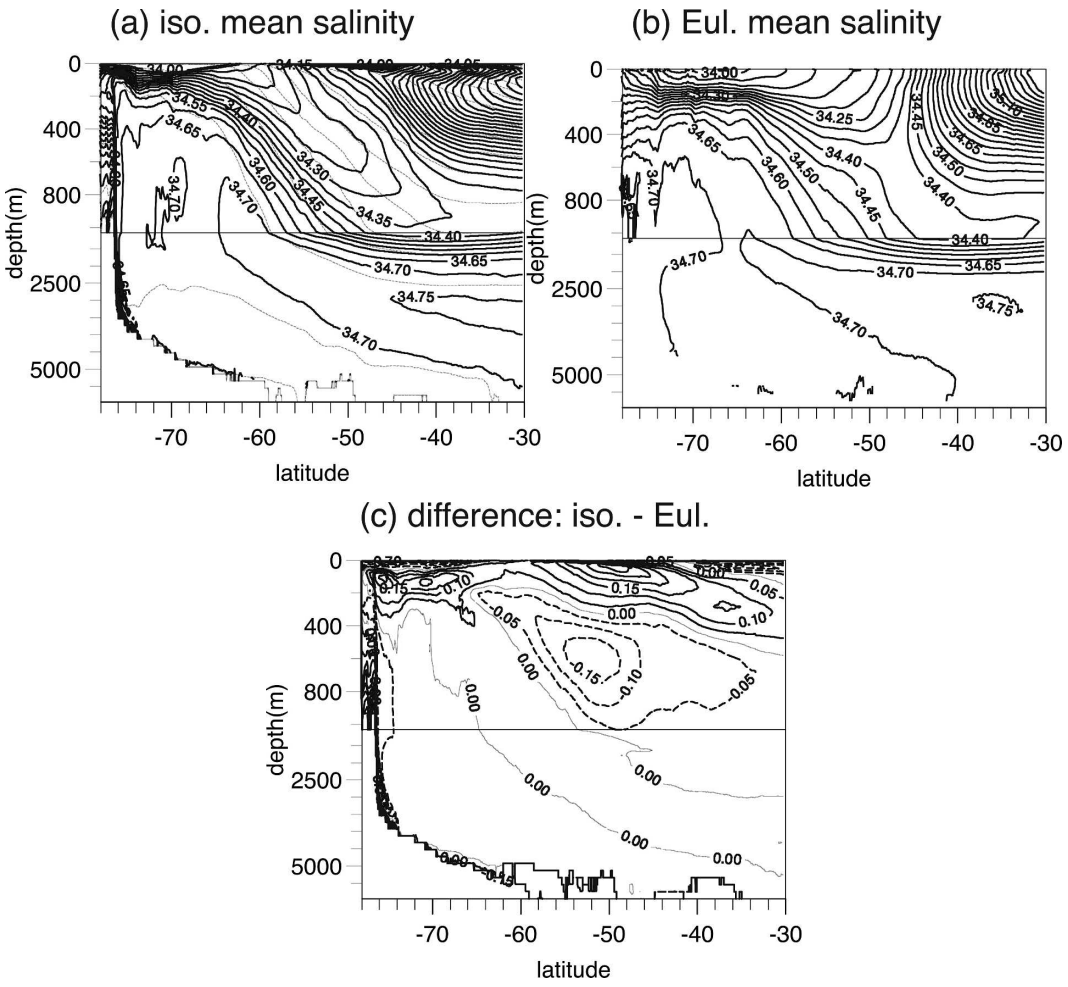

FIG. 3. As in Fig. 2, but for salinity. The contour interval is 0.05 psu.

and freshening. The equatorward return flow is at about 400–800 m, which forms intermediate water with low salinity ($S < 34.35$). The 8-Sv circulation is much weaker than the 16 Sv found in previous studies (Döös and Webb 1994; Lee and Coward 2003). There is another counterclockwise cell of 12 Sv above 400 m. This cell seems unusual, although it has been found in Döös and Webb (1994) (using 6 yr of data in surface-referenced density coordinates) and McIntosh and McDougall (1996) (using 1 yr of data in neutral density coordinates). However, this cell was not apparent in Lee and Coward (2003), who also used σ_2 coordinates. We will not investigate this cell further in the present study.

The deep cell carries about 20 Sv. There is a poleward flow of the LCDW with high salinity ($S > 34.7$) at about 2500–3500 m. It ascends to about 200 m at 60°S and becomes denser at high latitudes as a result of surface cooling and brine rejection from sea ice formation. The resulting water is colder but slightly fresher than the LCDW and returns equatorward as the Antarctic Bottom Water (AABW). The 16-Sv circulation at high latitudes south of 60°S is a significant improvement as a result of including a sea ice component in the model. Models without sea ice are not able to represent properly the circulation south of 60° (e.g., Döös and Webb 1994; Lee and Coward 2003).

2) MEAN

To complete the picture, we also show the mean transport streamfunction resulting from the time-mean Eulerian flow $\bar{v}_{eu}$ in (3). We first calculate the time-mean Eulerian streamfunction at each point $\psi_{eu}(z) = \int_{bottom}^{z} \bar{v}|_z(z)\, dz$, where $\bar{v}|_z(z)$ is time-mean velocity averaged at constant z. This streamfunction ψ_{eu} is then remapped onto ρ using the time-mean height of isopycnals $\tilde{z}(\rho)$. Thus, we have $\psi_{eu}(\rho) = \psi_{eu}\,\tilde{z}(\rho)$ at each point.

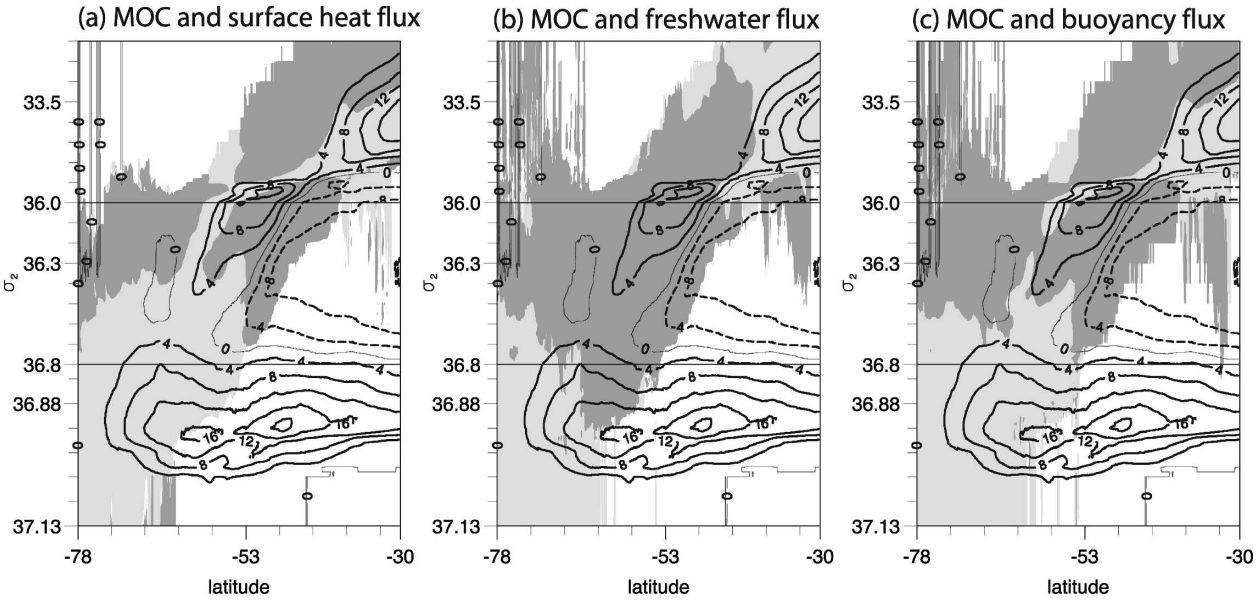

FIG. 4. Zonally integrated time-mean total transport streamfunction ψ (Sv) (4-Sv contour interval), superimposed is (a) surface heat flux, (b) freshwater flux, and (c) buoyancy flux. Dark shades are for flux gained by the ocean and light shades are for flux lost by ocean.

The streamfunction $\psi_{eu}(\rho)$ is then zonally integrated *along isopycnals* to obtain $[\psi_{eu}(\rho)]$. Last, we map $[\psi_{eu}(\rho)]$ back to z using the zonal and temporal mean height of isopycnals $[\tilde{z}]$ (Fig. 5c). Thus, we have the time-mean Eulerian transport streamfunction with zonal averaging taken along isopycnals. The advantage of this somewhat convoluted calculation is that by doing zonal averaging on isopycnals $[\psi_{eu}(\rho)]$ includes the standing eddies resulting from the zonal correlation between velocity and density. So, the difference between total streamfunction (Fig. 5a) and $[\psi_{eu}(\rho)]$ (Fig. 5c) is transient eddies (Fig. 5b, to be discussed in next section).

For comparison, the straightforward Eulerian streamfunction $\{\psi_{eu}(z)\}$, with zonal averaging taken on constant z, is shown in Fig. 5d. The difference between the Eulerian streamfunction (Fig. 5d) and $[\psi_{eu}(\rho)]$ (Fig. 5c) is standing eddies (not shown). The most notable feature is that standing eddies contribute to almost all the circulation at south of 65°S. This feature was absent in Lee and Coward (2003) because there was no sea ice in their model. In addition, it seems that the 12-Sv counterclockwise cell between 50° and 60°S above 400 m noted in the total streamfunction (Fig. 5a) is partly due to standing eddies (and partly due to transient eddies).

Note that the mean velocity $\bar{v}_{eu}$ in (3) is defined using $\psi_{eu}(\rho)$ as follows:

$$\frac{\partial \psi_{eu}(\rho)}{\partial \rho} = \bar{v}_{eu}(\rho)\bar{h}. \tag{9}$$

It should be stressed that $\bar{v}_{eu}(\rho)$ is not the same as the time-mean velocity averaged along isopycnals $\bar{v}(\rho)$, as previously used in Lee and Coward (2003). The main difference between them, which is important for our study, is that the vertically integrated transport of $\bar{v}_{eu}(\rho)$ gives the total transport, whereas $\bar{v}(\rho)$ does not,

$$\int_{\text{all }\rho} \bar{v}_{eu}(\rho)\bar{h}\, d\rho = \int_{\text{bottom}}^{\text{top}} \bar{v}|_z(z)\, dz = \int_{\text{all }\rho} \overline{vh}\, d\rho \neq \int_{\text{all }\rho} \bar{v}(\rho)\bar{h}\, d\rho. \tag{10}$$

5. Eddy transport

Over the Southern Ocean, the Antarctic Circumpolar Current (ACC) consists of a series of unstable fronts, generating vigorous baroclinic eddies. By extracting potential energy from the ACC and slumping isopycnals, baroclinic eddies induce an advective velocity flowing poleward near the surface and equatorward at depth.

The zonally integrated eddy transport streamfunction (resulting from transient eddies) is

$$\psi_{eddy}(y, \rho) = \int \int_{\rho}^{\rho_{max}} \bar{v}_{eddy}\bar{h}\, d\rho\, dx,$$

where $v_{eddy} = \hat{v} - \bar{v}_{eu}$ is defined as in (3) and $\bar{v}_{eu}$ is given by (9). This is shown in σ_2 coordinates (Fig. 6a) and in depth coordinates after remapping (Fig. 5b). It shows

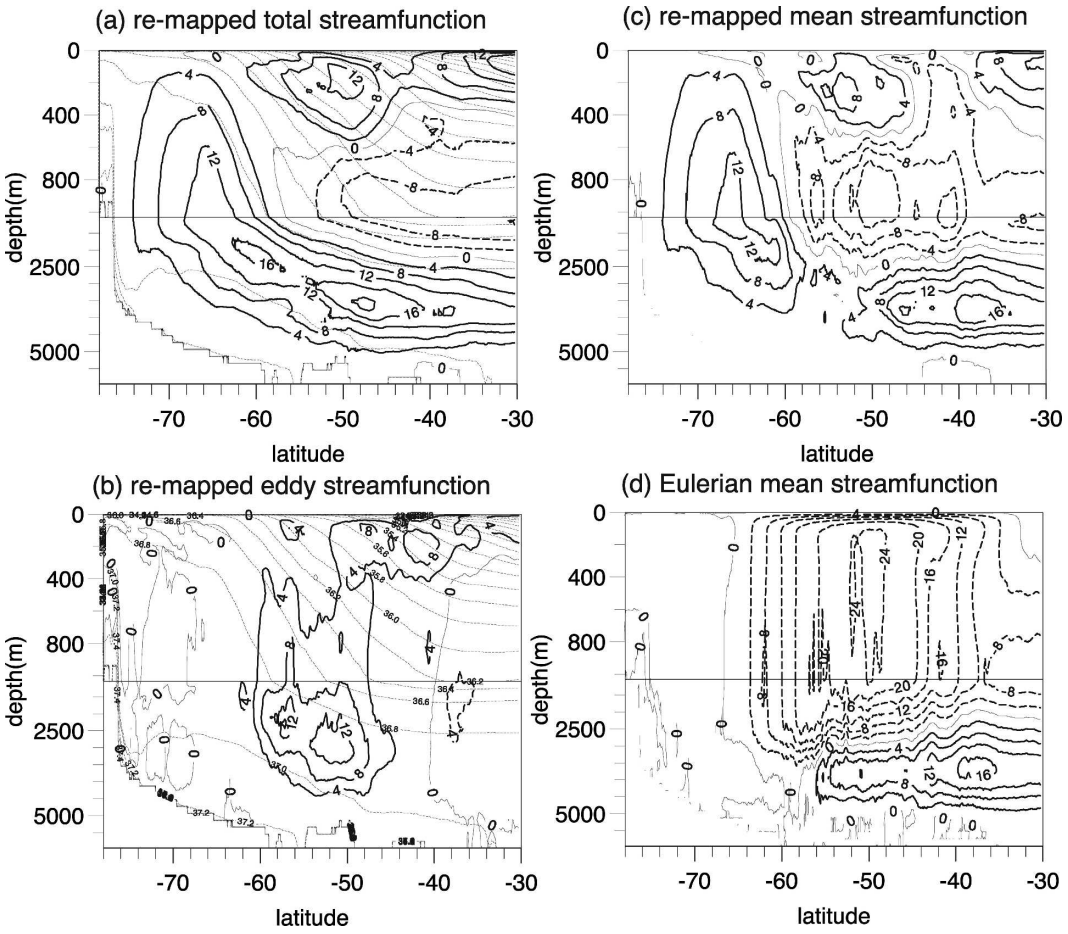

FIG. 5. Remapped transport streamfunction (Sv) as a function of depth using the mean depths of isopycnals for (a) the total and (b) the eddies; (c) $[\psi_{eu}(\rho)](z)$: time-mean Eulerian streamfunction with zonal averaging taken on isopycnals and then remapped back to z (see text), and (d) Eulerian streamfunction $\{\psi_{eu}(z)\}$ with both time and zonal averaging on z. The mean depths of isopycnals $[\tilde{z}]$ are superimposed (thin dashed lines) in (a) and (b) with density contour interval 0.2 kg m^{-3}.

an overturning cell between 50° and 60°S with a maximum of 15 Sv at 3000 m. The twin peaks of maximum transport can be attributed to the sub-Antarctic and polar fronts. At 43°S, there is another eddy-induced cell with a maximum of 12 Sv above 400 m. This cell is associated with the subtropical front.

For the cell centered at 55°S, the poleward eddy flow mainly occurs in the intermediate density classes $36 < \sigma_2 < 36.88$ at 400–2500 m, and very little occurs above 200 m. The poleward eddy transport may be compared with the wind-driven Ekman flow, which is binned into density classes and shown as a streamfunction (Fig. 6c). The Ekman transport is equatorward and the depth-integrated transport reaches a maximum of 27 Sv at 48°S (Fig. 6e). The latitudinal maximum value of the eddy transport streamfunction appears to be nearly half of the Ekman transport (Fig. 6e). However, this does not indicate eddies cancelling nearly one-half of the Ekman transport because Ekman flow occurs in the density classes much lighter than those for the poleward eddy flow. On the other hand, the equatorward eddy flow occurring below 2500–3000 m does contribute more than half of the equatorward transport of the AABW.

We should emphasize that the eddy velocity $\overline{v}_{eddy}$, which is equivalent to the quasi-Stokes velocity of McDougall and McIntosh (2001), is not the same as the bolus velocity $\overline{v}_{bolus} = \hat{v} - \overline{v}$. For heat transport, it is crucial that we use $\overline{v}_{eddy}$ rather than $\overline{v}_{bolus}$, because the former has a zero barotropic transport whereas the latter does not [cf. Eq. (10)]. To confirm this, we plot the bolus streamfunction associated with bolus velocity (Fig. 6b). In broad terms, the two streamfunctions are similar except that the bolus streamfunction is slightly weaker for the cell centered at 53°S but stronger for the one centered at 40°S. Also, the bolus streamfunction is

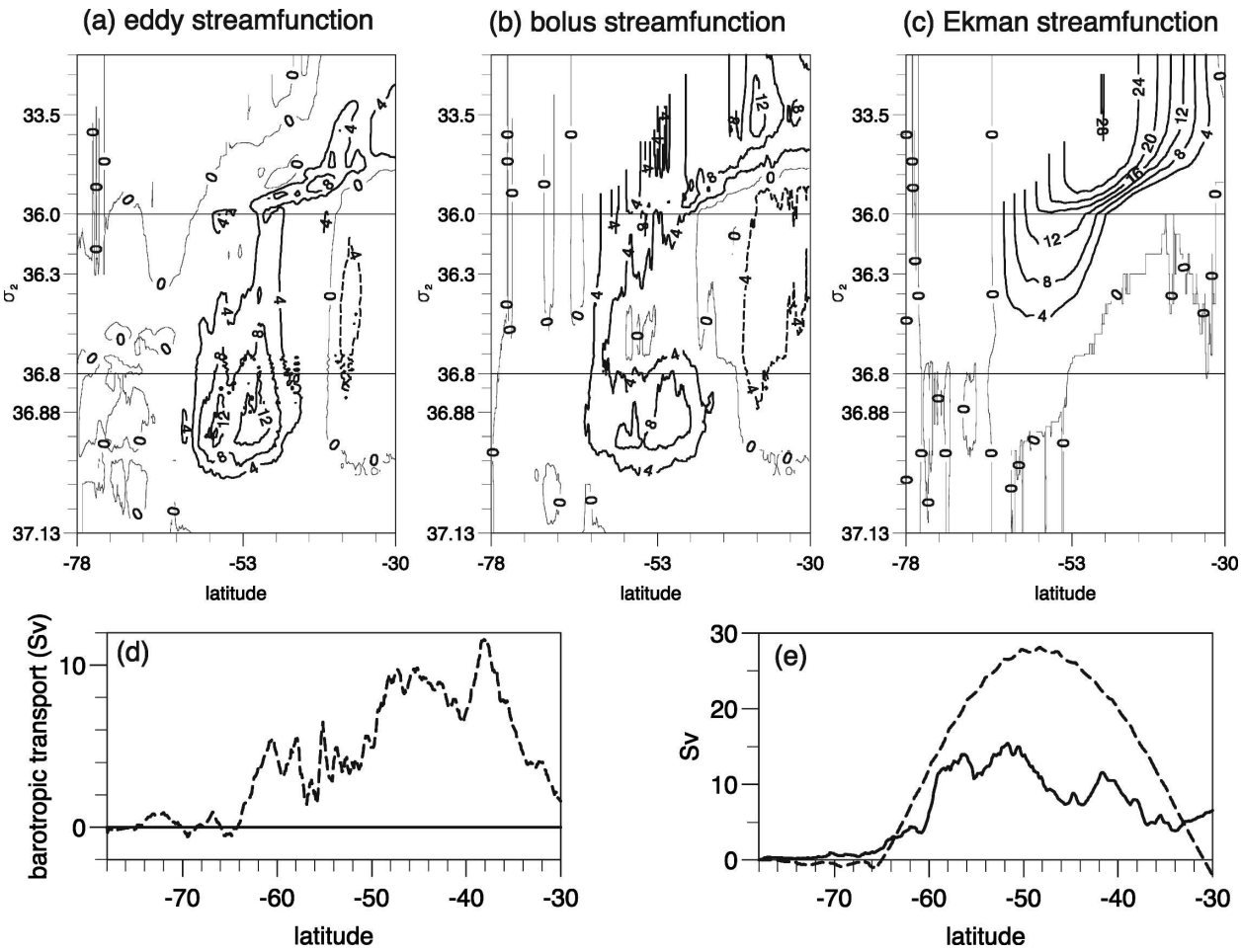

FIG. 6. Transport streamfunctions (Sv), with contour interval 4 Sv, calculated from (a) eddy velocity $\bar{v}_{\text{eddy}}$, (b) bolus velocity $\bar{v}_{\text{bolus}}$, and (c) Ekman velocity; (d) the barotropic transport for bolus velocity (dashed line) and eddy velocity (solid line); and (e) Ekman transport (dashed line) and the latitudinal maximum of eddy transport streamfunction (solid line).

noisier in the lighter density layers and does not close at the surface. It can be seen clearly from the barotropic transport (Fig. 6d) that ψ_{eddy} nearly vanishes ($\sim 10^{-3}$ Sv) at the surface, whereas the bolus streamfunction at the surface is 5 Sv at 60°S and up to 11 Sv at 38°S. This is the reason why $\bar{v}_{\text{eddy}}$ is more appropriate than $\bar{v}_{\text{bolus}}$, especially for the heat transport.

The eddy transport may be compared with other estimates. The earlier version of OCCAM at ¼° resolution had an maximum 6-Sv eddy transport (calculating from $\bar{v}_{\text{bolus}}$) (Lee and Coward 2003). Olbers and Ivchenko (2001) found a maximum of 25 Sv at 3000 m in the Parallel Ocean Program (POP) model. Using climatological values and eddy parameterization, Speer et al. (2000) suggested an eddy transport of 5–10 Sv in the UCDW using eddy diffusivity of 500–1000 $\text{m}^2\ \text{s}^{-1}$. Karsten and Marshall (2002) estimated 28 Sv using a different climatological values and altimeter-derived eddy diffusivity. Based on large-scale heat and freshwater budgets, Bryden and Cunningham (2003) alternatively deduced 28 Sv of southward flow and attributed it to eddies.

a. Heat transport

For heat transport, we take τ to be the temperature and zonally integrate (5). The meridional eddy heat transport is separated into two components: the advective heat transport $[\bar{v}_{\text{eddy}}\hat{T}\bar{h}]$ and the diffusive heat transport $[\widehat{v''T''h}]$.

Figure 7a shows the vertically and zonally integrated eddy heat transport. The eddy diffusive heat transport is poleward for all latitudes (dash-dotted line in Fig. 7a). This is because water is warmer toward the equator, and down-gradient diffusion leads to poleward diffusive heat transport. The diffusive transport is an order of 0.05–0.1 PW between 46° and 60°S and reaches a maximum of 0.15 PW at 42°S.

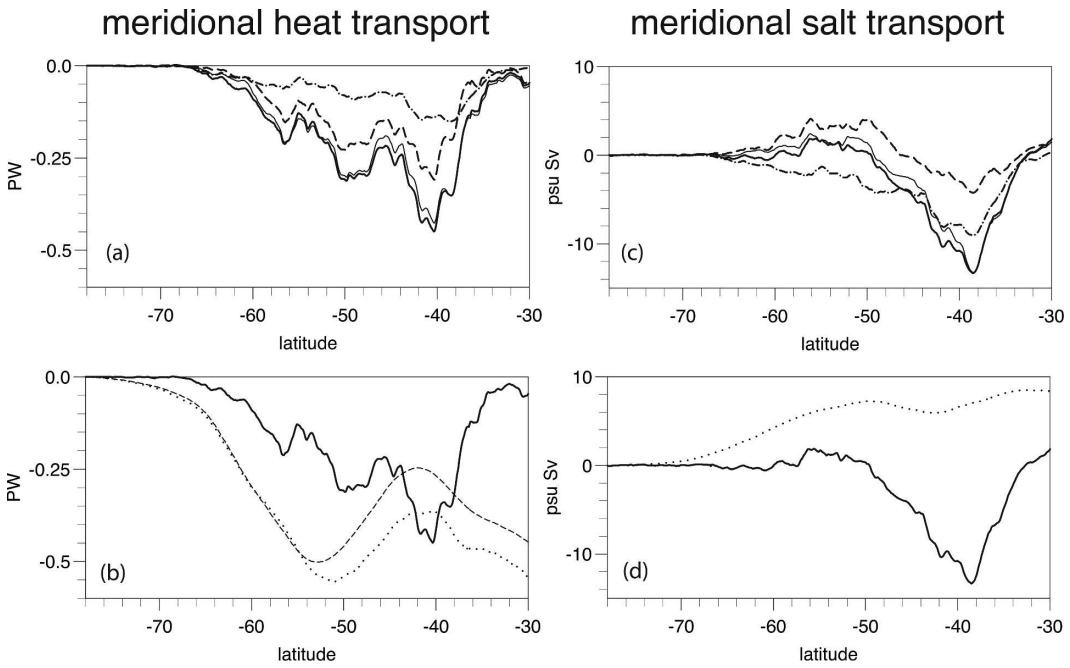

FIG. 7. (a) Vertically and zonally integrated meridional eddy heat transport (PW): advective transport $\bar{v}_{\text{eddy}}\hat{\bar{T}}\bar{h}$ (dashed line), diffusive transport $\widehat{\overline{v''T''}\bar{h}}$ (dash–dotted line), sum of advective transport and diffusive transport (thick solid line), and Eulerian eddy heat transport $\overline{v'T'}|_z$ (thin solid line); and (b) heat budget: sum of advective and diffusive transport (thick solid line) as in (a), where the total heat transport $\overline{vhT}$ (dotted line) and the cumulative surface heat flux are integrated from south to a given latitude (thin dashed line), and (c) as in (a) for eddy salt transport (psu Sv). (d) Same as (b), but for salt budget.

To predict the direction of eddy advective heat transport, we use the eddy transport streamfunction and mean temperature (Figs. 2a and 5b). In the surface layer poleward eddy flow brings warmer water toward the pole and in the deeper layer equatorward eddy flow takes colder water away from the pole, leading to a net poleward eddy heat transport. This is similar to the illustration in the schematic of Fig. 1. Although the direction of advective heat transport cannot be uniquely defined in each individual isopycnic layer, the vertically integrated eddy advective heat transport can because the vertical integral of eddy mass transport is nearly zero at each point (this is why we use $\bar{v}_{\text{eddy}}$ rather than $\bar{v}_{\text{bolus}}$). The advective eddy heat transport is about 0.1–0.2 PW over 46°–60°S and reaches a maximum of 0.3 PW at 42°S (dashed line in Fig. 7a). The large value of eddy advective (and diffusive) heat transport around 42°S is due to the Agulhas eddies and the Agulhas return current, which form part of the northern boundary of the ACC.

Combining the advective and diffusive transports gives a total eddy heat transport of about 0.1–0.3 PW over 50°–60°S and a maximum transport of 0.45 PW at 42°S (thick solid line in Figs. 7a and 7b). South of 44°S, eddies contribute to about half of the total poleward heat transport (Fig. 7b, dotted line). Near 40°S, poleward eddy heat transport compensates the equatorward mean heat transport and so the total heat transport is less poleward than the eddy heat transport itself.

There are estimates of eddy heat transport based on current meter data at few locations in the ACC. Bryden (1979) estimated eddy heat transport at Drake Passage and extrapolated over the entire latitude to give 0.75 PW. Phillips and Rintoul (2000) found a large heat transport from a mooring array to the south of Australia and, by extrapolation, estimated 0.9 PW of eddy heat transport across streamlines. These values are sufficiently large to balance heat loss to the atmosphere. Using a large-scale budget, de Szoeke and Levine (1981) estimated a 0.4 ± 0.3 PW eddy heat transport across the ACC and Gorden and Owens (1987) estimated 0.5 PW. Stammer (1998) estimated the eddy heat transport using time-mean temperature and altimeter-derived eddy diffusivity to obtain 0.3 PW at 40°S. From an eddy-permitting model, Jayne and Marotzke (2002) reported an eddy heat transport of 0.6 PW at 40°S.

The cumulative surface heat flux, integrated from the pole to a given latitude, is shown in Fig. 7b. South of 50°S, the total heat transport balances the cumulative surface heat flux, which is an indication of small heat

storage there. At 55°S, the two curves start to deviate, but maintain the same discrepancy throughout the rest of the latitudes. This indicates heat storage becoming significant around 55°S. In all respects, the total heat transport and the cumulative surface flux vary similarly as a function of latitude.

South of 50°S, the balance is between the heat transport convergence and surface cooling, that is, the cumulative heat loss to the atmosphere is replenished by the poleward heat transport and half of the poleward heat transport is due to eddies. To the north of 50°S, the balance is more complicated. Within the band between 40° and 50°S, the surface heat flux is into the ocean. This surface heating is balanced by the divergence of total heat transport with more poleward heat transport at 50°S than at 40°S. But, the eddy heat transport over the same latitude band is convergent with more poleward heat transport at 40° than at 50°S. Thus, the surface heating is *not* balanced by eddies transporting heat out of the region. Instead, it is the heat transport by time-mean Eulerian flow that balances the surface heating.

b. Salt transport

Like the eddy heat transport, the eddy salt transport is separated into eddy advective transport $[\overline{\mathbf{u}}_{\text{eddy}}\hat{\bar{S}}\bar{h}]$ and eddy diffusive transport $[\widehat{\mathbf{u}''S''}\bar{h}]$.

The mean salinity field is more complex than the mean temperature field because of the presence of the relatively fresh AAIW and the relatively salty LCDW (Fig. 3a). However, it is still true that fresher water is on the poleward side following isopycnal surfaces. So, down-gradient diffusion implies that the eddy diffusive salt transport is poleward. The vertically and zonally integrated eddy diffusive salt transport is about 3–5 psu Sv poleward and has a maximum of 10 psu Sv at 40°S (dashed–dotted line in Fig. 7c).

The eddy advective salt transport needs closer examination because the vertical distribution of salinity is not monotonic. North of 50°S the fresh AAIW is sandwiched between the saltier light water above and saltier dense water below. From the eddy mass transport plot in Fig. 5b and mean salinity in Fig. 3a, we see that between 45° and 60°S eddies transport relatively freshwater poleward in the lighter surface water and transport relatively salty water equatorward in the denser deep layer. Thus, the salt transport resulting from eddy advection should be equatorward as expected from the schematic in Fig. 1. The diagnosed eddy advective salt transport is indeed 3–5 psu Sv equatorward over 45° and 60°S (dashed line in Fig. 7c).

Farther north between 38° and 45°S, the eddy-overturning circulation occurs in the much lighter density classes above 400 m. For that density range in the region, the water is saltier at the surface than below. So, eddies carry salty water poleward and fresher water equatorward, leading to poleward salt transport around 38°–45°S (dashed line Fig. 7c). This is also consistent with the schematic in Fig. 1 with the reversed vertical salinity gradient. Thus, the direction of advective salt transport can be poleward (at lower latitudes) or equatorward (at higher latitudes). In each case the transport direction agrees with the large-scale vertical gradient of salinity, as in our simple schematic.

Thus, while the eddy diffusive salt transport is poleward for all latitudes (south of 30°S), the eddy advective salt transport can be either equatorward or poleward. This is in contrast to the eddy heat transport where eddy advective and diffusive heat transports are both poleward for all latitudes. This means that eddy advective transport can oppose eddy diffusive transport for salinity but not for temperature. This has consequences for the net eddy contribution to the salt budget.

To the south of 50°S, nearly all the eddy advective transport is cancelled by the diffusive transport (thick solid line in Figs. 7c and 7d). The net eddy salt transport contributes only 1–2 psu Sv over 50°–60°S where the total salt transport is about 7–9 psu Sv (dotted line in Fig. 7d). Thus, south of 50°S the net eddy contribution to the salt budget is relatively small in comparison with the eddy contribution to the heat budget. To the north of 50°S, the eddy advective and diffusive salt transports are both poleward, and so the net eddy salt transport reaches 13 psu Sv poleward at 40°S. However, the total salt transport is about 7 psu Sv equatorward. (Note that there should be no total salt transport if the model is in steady state and so the equatorward total salt transport indicating that model is still evolving). Hence, the Eulerian mean flow provides equatorward salt transport of 20 psu Sv and eddies cancel more than one-half of it.

c. Comparison with Eulerian eddy transport

The aim of this study is to emphasize that eddy transport of tracer on isopycnals has an advective part and a diffusive part. We have demonstrated in terms of heat and salt transports that the two eddy processes can have very different effects on tracers depending on the large-scale tracer distribution. In contrast, in the Eulerian framework the eddy transport of tracer is $v'\tau'$ and there is no unique way of separating out a component on isopycnal surfaces (Nurser and Lee 2004b). Here, we discuss briefly the difference between isopycnic eddy

transport and the Eulerian eddy transport in a vertically and zonally integrated sense.

The Eulerian eddy heat transport is

$$\overline{v'T'}|_z = \overline{vT}|_z - \overline{v}|_z\overline{T}|_z, \tag{11}$$

where the overbar $|_z$ is the time averaging on z and the prime is the deviation from the time mean. The vertically and zonally integrated Eulerian eddy transport is shown in Fig. 7a (thin solid line). It is very close to the total isopycnic eddy heat transport (advective and diffusive combined) (thick solid line in Fig. 7a).

To explain this, we take the total meridional eddy heat transport on isopycnals from (4)

$$\overline{v}_{\text{eddy}}\hat{T}\overline{h} + \widehat{\overline{v''T''h}} = \overline{vhT} - \overline{v}_{\text{eu}}\hat{T}\overline{h}. \tag{12}$$

Integrate (11) and (12) vertically. The total heat transport (the first terms on the rhs of both equations) is the same because the total heat transport does not depend on the coordinate used ($\int\overline{vhT}\,d\rho = \int\overline{vT}|_z\,dz$). However, the mean heat transport varies depending on which mean temperature is used—the isopycnic mean temperature $\hat{T}$ or the Eulerian mean temperature $\overline{T}$.

Although, as discussed in section 4a, the two mean temperatures $\hat{T}$ and $\overline{T}$ differ considerably, it turns out the mean mass transport (Fig. 5c) is such that the mean heat transport is not much affected. At 55°S between 400 and 1000 m, the fact that $\hat{T}$ is cooler than $\overline{T}$ has no net effect because the mean mass transport is equatorward around 400–800 m and poleward around 800–1000 m. In a similar way, $\hat{T}$ is warmer than $\overline{T}$ above 400 m but there is poleward transport above 200 m and equatorward transport between 200–400 m. In terms of vertically integrated heat transport, the mean mass transport effectively cancels the differences in two mean temperatures.

Similar arguments also apply to the eddy salt transport. The vertically and zonally integrated Eulerian eddy salt transport is close to that from the isopycnic calculation (thin and thick solid lines in Fig. 7c).

6. Advective versus diffusive transports

We have shown that the direction of advective transport and diffusive transport is determined by the eddy transport velocity and large-scale gradient of tracer as illustrated by the simple schematic in Fig. 1. In this section, we would like to extend the idea further by allowing the eddy transport velocity to be parameterized.

Using the GM90 eddy parameterization, the eddy advective velocity $\overline{v}_{\text{eddy}}$ can be expressed as

$$\overline{v}_{\text{eddy}} = -\frac{\partial}{\partial z}(\kappa_{\text{GM}}\Gamma_\rho), \tag{13}$$

where κ_{GM} is the GM90 eddy diffusivity and Γ_ρ is the isopycnal slope.

The diffusive transport can be rewritten in z coordinates

$$\begin{aligned}-\kappa_\tau\frac{\partial\hat{\tau}}{\partial y}\bigg|_\rho\overline{h} &= -\kappa_\tau\left(\frac{\partial\hat{\tau}}{\partial y}\bigg|_z + \frac{\partial\hat{\tau}}{\partial z}\frac{\partial z}{\partial y}\bigg|_\rho\right)\overline{h}\\ &= -\kappa_\tau\left(-\frac{\partial z}{\partial y}\bigg|_{\hat{\tau}} + \frac{\partial z}{\partial y}\bigg|_\rho\right)\frac{\partial\hat{\tau}}{\partial z}\overline{h}\\ &= \kappa_\tau(\Gamma_\tau - \Gamma_\rho)\frac{\partial\hat{\tau}}{\partial z}\overline{h},\end{aligned} \tag{14}$$

where Γ_τ is the slope of tracer.

We will use the scaling analysis for a two-layer fluid as before. From (13), we assume the isopycnal slope Γ_ρ vanishes at the surface and at bottom. Thus, the vertically integrated advective transport can be scaled as

$$V(\tau_u - \tau_l)H = \kappa_{\text{GM}}(\tau_u - \tau_l)\Gamma_\rho. \tag{15}$$

From (14), the vertically integrated diffusive transport can be scaled as

$$\kappa_\tau(\Gamma_\tau - \Gamma_\rho)(\tau_u - \tau_l), \tag{16}$$

where κ_τ is taken as the scale of vertically averaged isopycnic diffusivity.

From (15) and (16), the ratio of diffusive transport to advective transport scales as

$$\mathcal{R}(\tau) = \frac{\text{eddy diffusive}}{\text{eddy advective}} \sim \frac{\kappa_\tau(\Gamma_\tau - \Gamma_\rho)}{\kappa_{\text{GM}}\Gamma_\rho} = \frac{\kappa_\tau}{\kappa_{\text{GM}}}\left(\frac{\Gamma_\tau}{\Gamma_\rho} - 1\right). \tag{17}$$

From this simple scaling, we can determine the relative sign of eddy advective and diffusive transports.

The relative sign

Assuming the eddy diffusivities are positive, the sign of the ratio $\mathcal{R}$ in (17) is determined by whether Γ_τ/Γ_ρ is greater or less than 1.

Case I is $\Gamma_\tau/\Gamma_\rho > 1$. In this case, eddy advective and diffusive transports have the same direction. This occurs when the two slopes are inclined in the same direction and tracer slope is steeper than isopycnal slope (left two panels in Fig. 8). The eddy advective and diffusive transports can be either both poleward or both equatorward. Assume that isopycnals rise poleward (as before in Fig. 1). If the tracer increases upward then both eddy advective and diffusive transports are poleward (top left panel in Fig. 8). Otherwise, both eddy advective and diffusive transports are equatorward (bottom left panel in Fig. 8).

Case II is $\Gamma_\tau/\Gamma_\rho < 1$. In this case, eddy advective and diffusive transports have opposite directions. This occurs when the two slopes are inclined in the opposite direction or when the two slopes are inclined in the

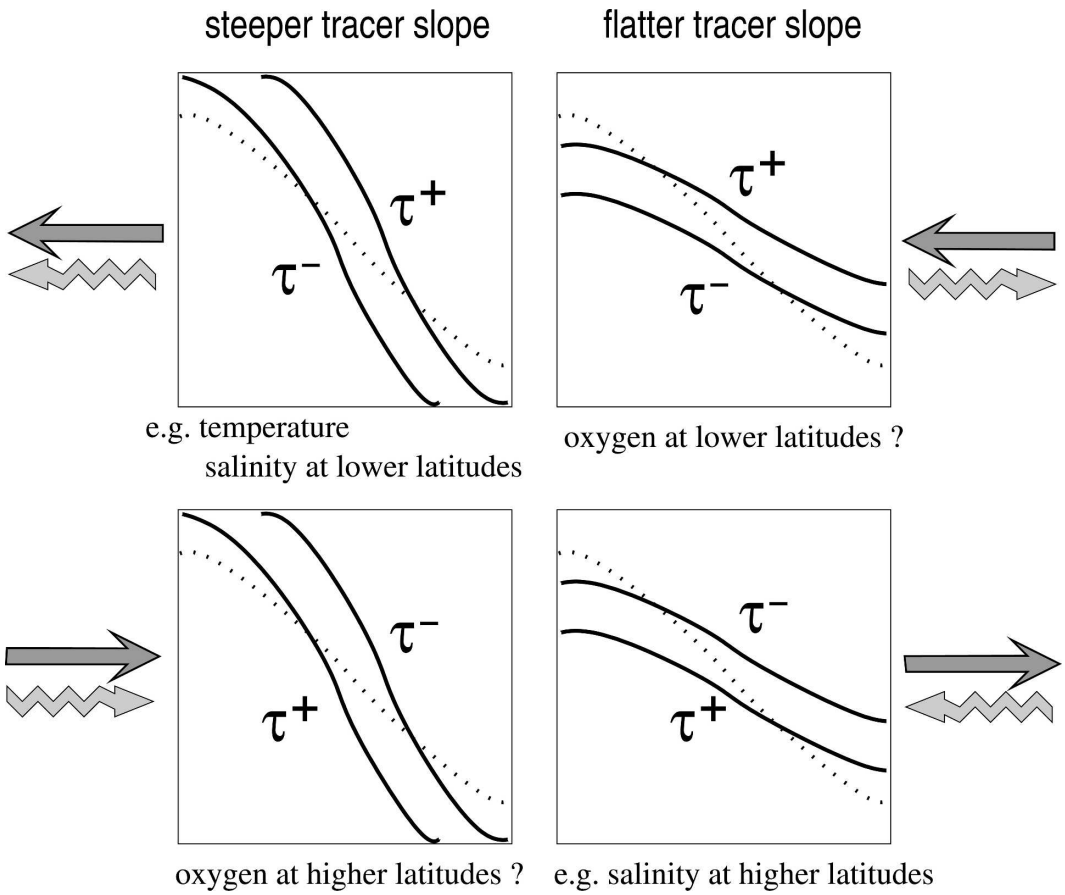

FIG. 8. Schematic illustrating that the directions of eddy advective and eddy diffusive transports are determined by the relative slopes of tracers and isopycnals. When the tracer slope is steeper (or flatter) than the isopycnal slope, the eddy advective transport has the same (or opposite) direction to the eddy diffusive transport, as in the left two panels (or the right two panels). The direction of each eddy transport is determined by the vertical gradient of tracer. Straight shaded arrows indicate eddy advective transport and curved shaded arrows indicate eddy diffusive transport. Dotted lines are for isopycnals and solid lines are for tracers. High tracer is denoted by τ^+ and low tracer by τ^-.

same direction with tracer slopes flatter than isopycnal slopes (two right panels in Fig. 9 show the case when the two slopes are inclined in the same directions). As in case I, the direction of each eddy transport is determined by how the tracer varies vertically.

Case III is $\Gamma_\tau/\Gamma_\rho = 1$. This implies $\mathcal{R} = 0$, and so there is no eddy diffusive transport. This is consistent with the fact that if the two slopes are the same, then tracer is uniform on the isopycnal and so there is no eddy diffusion of tracer along isopycnals.

We can check the above criteria against the eddy transport of temperature and salinity. The mean temperature field in Fig. 2a shows that temperature contours closely follow isopycnals in most places. This is because density is mainly determined by temperature. When temperature contours do cross isopycnals (around 54°S at 800 m and north of 40°S above 200 m), the temperature slopes are often steeper than isopycnal slopes. This is because warmer water is on the equatorward side as well as near the surface. Hence, $\Gamma_{\hat{T}}/\Gamma_\rho > 1$ and $\hat{T}$ increases upward, which is like the top-left panel of the schematic in Fig. 8. Thus, eddy advective and diffusive heat transport are expected to be both poleward, as predicted by the schematic, and agree with our model diagnosis shown earlier in Fig. 7a.

For salinity, we first examine the mean salinity field (Fig. 3a) between 50° and 60°S. Here, the salinity contours often cross isopycnals at all depths and salinity slopes are in general less steep than the isopycnal slope. For example, the $\hat{S} = 34.7$ water (LCDW) is found in denser layers on the poleward side and in the lighter layer on the equatorward side. This is due to the fact that deep water is saltier than the surface water and as the LCDW moves poleward it becomes fresher resulting from the surface freshening from ice melt. So, $\Gamma_{\hat{S}}/\Gamma_\rho < 1$ and salinity decreases upward. This is like the

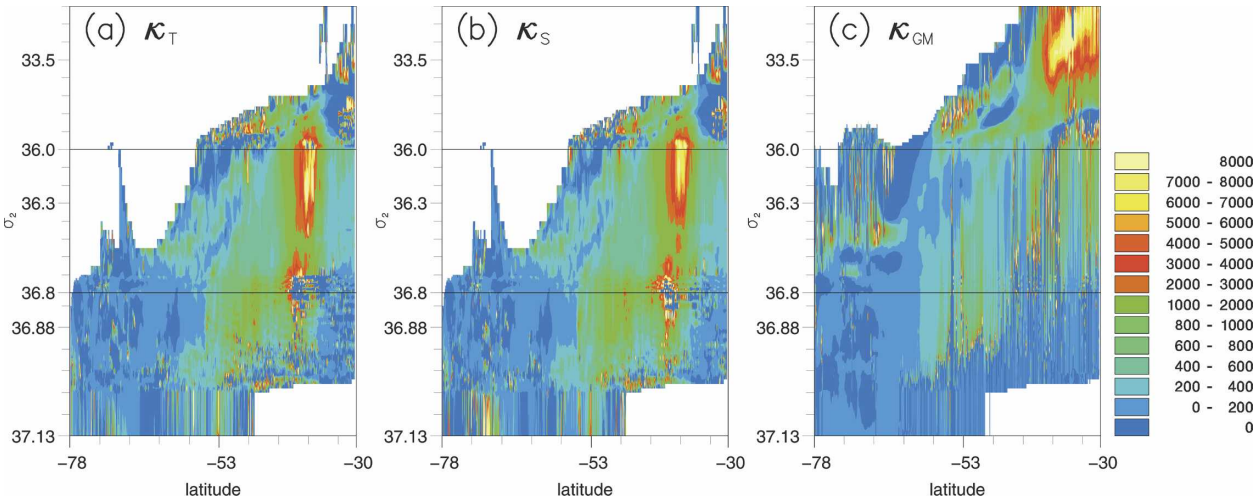

FIG. 9. Eddy diffusivity ($m^2\ s^{-1}$) for (a) temperature, (b) salinity, and (c) eddy transport velocity. Here (a) and (b) do not include layers that ever reach the surface.

case depicted in the bottom-right panel of the schematic in Fig. 8. This means that eddy advective and diffusive salt transport must have opposite directions with the advective transport equatorward and diffusive transport poleward. This is also confirmed by the model diagnosis in Fig. 7c.

For latitudes between 40° and 50°S, eddy mass transports are strongest near the surface (Fig. 5b), and so we will focus on the salinity field above 800 m. Between 200 and 400 m, salinity contours are steeper than isopycnal slopes (Fig. 3a). This is because as water moves equatorward it becomes saltier resulting from evaporation, and also salty water lies above the freshwater. Thus, $\Gamma_{\hat{S}}/\Gamma_\rho > 1$ and salinity increases upward. This is like the top-left panel in Fig. 8. So, we have the poleward advective and diffusive salt transports, which is consistent with the diagnosis in Fig. 7c. Note that there is a hint of salinity slope in the opposite sign to the isopycnal slope above 100–200 m. Because this lies within the mixed layer, our argument in case II does not apply to this depth range.

In summary, using a simple scale analysis and GM90 parameterization, we argue that the relative directions of eddy advective and diffusive transports may be determined from the relative slopes of tracers and isopycnals. Although our argument based on a two-layer fluid seems too simplified for a continuously stratified fluid, the diagnosis from the model agrees remarkably well with the predictions.

7. Eddy diffusivity

One of the main objectives of this paper is to stress that tracer transport by eddy advection is a fundamentally different process from that by eddy diffusion. In climate modeling, one must have confidence that eddy processes are accurately represented. Standard practice at present is to parameterize the eddy advective transport velocity as in GM90 and the eddy diffusive transport of tracer as down the mean tracer gradient along isopycnals (Griffies 1998). However, many climate models use the same diffusivity for eddy advective transport velocity and for eddy diffusion of tracers. In this section, we diagnose eddy diffusivities from the model and compare them.

The eddy isopycnic diffusivity for tracers should only be diagnosed for the interior isopycnic layers, and so we exclude the transport in the surface mixed layer where eddies mix across isopycnals. At each point we define $\sigma_{2\max}(x, y)$ to be the densest isopycnal that ever reaches the surface over the 5-yr diagnosis period. Each water column is then separated into two portions with the interior portion containing isopycnals denser than $\sigma_{2\max}(x, y)$ and the surface portion containing the remaining isopycnals. Thus, the surface portion has those isopycnals that have surfaced at least once and the interior portion has those isopycnals that never reach the surface. The diffusive transport in the surface portion accounts for nearly half of the total diffusive transport (not shown). Note that this is likely to overestimate the diffusive transport in the mixed layer because an isopycnic layer only needs to reach the surface once to be in the surface portion and such a layer may not be in the mixed layer all the time.

Thus, the isopycnic eddy diffusivities for temperature and salinity, κ_T and κ_S, respectively, are calculated for the interior portion only as follows:

$$\int (\widehat{u''\tau''}\,\overline{h})_{\text{interior}}\,dx = -\kappa_\tau \int \left(\frac{\partial \hat{\tau}}{\partial y}\,\overline{h}\right)_{\text{interior}} dx, \qquad (18)$$

where we assume the eddy diffusivity is constant at each latitude. Figures 9a and 9b show that the diffusivities κ_T and κ_S are similar to each other. This is because along-isopycnal perturbations of temperature and salinity are correlated, as are the mean gradients of temperature and salinity. The largest diffusivity (more than 3000 $m^2\ s^{-1}$) occurs around 42°S, where the Agulhas eddies leads to relatively large diffusive transport seen earlier in Fig. 7. The next largest value (about 1000 $m^2\ s^{-1}$) is at 48°–50°S and is mainly due to large eddy diffusion near Kerguelen Plateau. Elsewhere, the diffusivity ranges between 300 and 600 $m^2\ s^{-1}$.

For eddy advective transport, one needs to parameterize the eddy transport velocity. We diagnose the eddy diffusivity following GM90:

$$\int \bar{v}_{\text{eddy}} \bar{h}\, d\rho\, dx = -\kappa_{\text{GM}} \int \frac{\partial \tilde{z}}{\partial y}\, dx, \tag{19}$$

where $\tilde{z}$ is the time-mean depth of isopycnals and κ_{GM} is assumed to be a function of latitude only. The eddy diffusivity κ_{GM} is diagnosed for all layers without separating into surface and interior portions. This is because the surface portion is needed to ensure zero total eddy transport at the surface.

The diffusivity for eddy transport velocity κ_{GM} (Fig. 9c) is more patchy in comparison with the diffusivity for temperature and salinity $\kappa_{T,S}$. In the lighter density layers $\sigma_2 < 33.6$, the large difference between κ_{GM} and $\kappa_{T,S}$ is due to the surface portion not being included in calculating isopycnic diffusivity for tracer. The background diffusivity for κ_{GM} is about 200–400 $m^2\ s^{-1}$, which is slightly lower than the background value for κ_{GM}. The largest contrast between them is that at 42°S, where κ_{GM} is much smaller than $\kappa_{T,S}$. The seems to reflect the fact that the eddy mass advective transport does not have the relatively large value at 42°S as the diffusive transport does (Figs. 6e and 7).

Our result suggests that when implementing eddy parameterizations in climate models, eddy diffusivity for tracer may differ considerably from the diffusivity for eddy transport velocity. This agrees with Treguier's (1999) diagnosis of a channel model, in which isopycnal diffusivities of passive scalar showed very different behavior from κ_{GM} (see her Fig. 10), with κ_{GM} about 200 $m^2\ s^{-1}$ and passive diffusivities reaching nearly 2000 $m^2\ s^{-1}$.

Recently, Marshall et al. (2006) calculated effective eddy diffusivity at surface using passive tracers in a 1/20° resolution model. Their results are not strictly comparable to ours because they focused on the surface. However, they also have high-value diffusivity of 2000–3000 $m^2\ s^{-1}$ at the equivalent latitude of 40°S. This is smaller than our $\kappa_{T,S}$ but larger than κ_{GM} at the similar latitude. At other latitudes, their diffusivity at surface is about 1000 $m^2\ s^{-1}$, which is slightly larger than ours in the interior.

8. Conclusions

The tracer transport by baroclinic eddies plays an important role in the large-scale tracer budget. The aim of our study is to highlight the two eddy processes involved: eddy advective transport and eddy diffusive transport. Lee and Williams (2000) demonstrated that, in an isopycnal layer, eddy advective transport and eddy diffusive transport can either enhance or oppose each other, and whether eddy advection or eddy diffusion dominates depends on the lifetime of tracers. In this study, we address the vertically integrated eddy tracer transport. The basic idea is that the direction of eddy advective transport is governed by the large-scale across-isopycnal vertical tracer gradient and eddy diffusive transport is governed by large-scale along-isopycnal meridional tracer gradient, as illustrated in the schematic in Fig. 1.

For temperature, the large-scale spatial distribution is relatively simple: warmer at the surface than at depth, and warmer at the equator than at the pole. Consequently, eddy advective and diffusive heat transports are both poleward, and so eddy advection and eddy diffusion enhance each other. In contrast, the distribution of salinity is more complicated because of the presence of the fresh AAIW at middepth and the salty LCDW at greater depth. As a result, north of 50°S eddy advective and diffusive transport of salt are both poleward. However, south of 50°S eddy advective and diffusive transport are in the opposite direction, and so there is a competition between eddy advection and eddy diffusion. Thus, unlike eddy heat transport, eddy advection and eddy diffusion of salt can enhance (at lower latitudes) or oppose (at higher latitudes) each other. This explains why at higher latitudes eddies contribution to the salt budget is relatively less significant than they do to the heat budget.

We generalize the basic idea by writing eddy transport velocity in the form of the GM90 parameterization. In doing so, the relative direction of eddy advective and diffusive tracer transports can be determined simply from the relative slopes of tracers and isopycnals. When the two slopes are inclined in the same way, and if tracer slopes are steeper (or flatter) than isopycnal slopes, then eddy advection and diffusion have the same (or opposite) direction, as in the schematic of Fig. 8. Thus, we argue that the reason that eddy advective and diffusive transport of heat have the same direction

is because temperature slopes are steeper than the isopycnal slopes. Similar arguments apply to the eddy salt transports at lower latitudes where salinity slopes are steeper than isopycnal slopes. However, at higher latitudes salinity slopes are flatter than isopycnal slopes, hence the opposite direction between eddy advective and diffusive salt transport.

The diagnosis of our high-resolution (1/12°) eddy-resolving model agrees remarkably well with the simple scaling analysis. The results seem robust, because we have also obtained qualitatively similar results from the same model at a coarser resolution of 1/4°.

Temperature and salinity are just two examples presented. From the schematic in Fig. 8, we can predict the direction of eddy transport for other tracers such as oxygen, nitrate, silicate, etc. For example, the oxygen section along the Greenwich meridian in the Weddell Gyre shows that the oxygen minimum lies close to the UCDW layers and the oxygen (like the salinity) maxima lie within the LCDW layers (Orsi et al. 1995). Furthermore, oxygen is generally higher toward the pole because of deep ventilation. We may predict that at higher latitudes eddy advective and diffusive oxygen transports are both equatorward, as in the bottom left panel in Fig. 8. However, at lower latitudes, the two components of eddy oxygen transport are in the opposite direction, as in the top right panel in Fig. 8.

For climate modeling, the eddy processes need to be appropriately represented. From the diagnosed eddy diffusivity, we found that the eddy diffusivity for tracers is different from that for eddy advective transport velocity. This questions the suitability of using the same eddy diffusivity for eddy advection and for eddy diffusion in climate modeling.

Acknowledgments. We thank Anne Marie Treguier and an anonymous reviewer for providing useful suggestions to improve the paper. Mei-Man Lee thanks Matthew England for arranging the visit to the University of New South Wales during which the idea in section 6 was born.

APPENDIX

Potential Density Classes

The 80 potential density classes (referenced at 1940 m) used for binning are as follows: 00.00, 10.00, 21.00, 24.00, 27.00, 30.00, 30.50, 31.00, 31.50, 32.00, 32.50, 33.00, 33.30, 33.60, 33.90, 34.20, 34.50, 34.80, 34.90, 35.00, 35.10, 35.20, 35.30, 35.40, 35.50, 35.60, 35.70, 35.80, 35.90, 36.00, 36.10, 36.20, 36.30, 36.40, 36.45, 36.50, 36.55, 36.60, 36.65, 36.70, 36.71, 36.72, 36.73, 36.74, 36.75, 36.76, 36.77, 36.78, 36.79, 36.80, 36.81, 36.82, 36.83, 36.84, 36.85, 36.86, 36.87, 36.88, 36.89, 36.90, 36.91, 36.92, 36.93, 36.94, 36.95, 36.96, 36.97, 36.98, 36.99, 37.00, 37.01, 37.02, 37.03, 37.13, 37.23, 37.33, 37.43, 37.53, 37.63, and 40.00.

REFERENCES

Aksenov, Y., 2002: The sea ice-ocean global coupled ARCICE project report part I: Description of dynamical thermodynamical sea ice model. SOC Research and Consultancy Rep. 103, 83 pp.

Bishop, J. K., W. B. Rossow, and E. G. Dutton, 1997: Surface solar irradiance from the International Satellite Cloud Climatology Project 1983–1991. *J. Geophys. Res.,* **102,** 6883–6910.

Boyer, T. P., S. Levitus, J. I. Antonov, M. E. Conkright, T. D. O'Brien, and C. Stephens, 1998: *Salinity of the Atlantic Ocean*. Vol. 4, *World Ocean Atlas 1998,* NOAA Atlas NESDIS 30, 166 pp.

Bryden, H. L., 1979: Poleward heat-flux and conversion of available potential-energy in Drake Passage. *J. Mar. Res.,* **37,** 1–22.

——, and S. A. Cunningham, 2003: How wind-forcing and air-sea heat exchange determine the meridional temperature gradient and stratification for the Antarctic Circumpolar Current. *J. Geophys. Res.,* **108,** 3275, doi:10.1029/2001JC001296.

Coward, A. C., and B. A. de Cuevas, 2005: The OCCAM 66 level model: Physics, initial conditions and external forcing. SOC Internal Rep. 99, 58 pp.

Danabasoglu, G., J. C. McWilliams, and P. R. Gent, 1994: The role of mesoscale tracer transports in the global ocean circulation. *Science,* **264,** 1123–1126.

de Szoeke, R. A., and M. D. Levine, 1981: The advective flux of heat by mean geostrophic motions in the Southern Ocean. *Deep-Sea Res.,* **28A,** 1057–1085.

Döös, K., and D. J. Webb, 1994: The Deacon cell and the other meridional cells of the Southern Ocean. *J. Phys. Oceanogr.,* **24,** 429–442.

Dukowicz, J. K., and R. J. Greatbatch, 1999: The bolus velocity in the stochastic theory of ocean turbulent tracer transport. *J. Phys. Oceanogr.,* **29,** 2442–2456.

Gent, P. R., and J. C. McWilliams, 1990: Isopycnal mixing in ocean circulation models. *J. Phys. Oceanogr.,* **20,** 150–155.

Gorden, A. L., and W. B. Owens, 1987: Polar oceans. *Rev. Geophys.,* **25,** 227–233.

Gouretski, V. V., and K. Jancke, 1996: A new hydrographic data set for the South Pacific: Synthesis of WOCE and historical data. WHP SAC Tech. Rep. 2, WOCE Rep. 143/96, 110 pp.

Griffies, S. M., 1998: The Gent–McWilliams skew flux. *J. Phys. Oceanogr.,* **28,** 831–841.

Held, I. M., and T. Schneider, 1999: The surface branch of the zonally averaged mass transport circulation in the troposphere. *J. Atmos. Sci.,* **56,** 1688–1697.

Hirst, A. C., S. P. O'Farrell, and H. B. Gordon, 2000: Comparison of a coupled ocean–atmosphere model with and without oceanic eddy-induced advection. Part I: Ocean spinup and control integrations. *J. Climate,* **13,** 139–163.

Jakobsson, M., N. Z. Cherkis, J. Woodward, R. Macnab, and B. Coakley, 2000: New grid of Arctic bathymetry aids scientists and mapmakers. *Eos, Trans. Amer. Geophys. Union,* **81,** 89.

Jayne, S. R., and J. Marotzke, 2002: The oceanic eddy heat transport. *J. Phys. Oceanogr.,* **32,** 3328–3345.

Kalnay, E., and Coauthors, 1996: The NCEP/NCAR 40-Year Reanalysis Project. *Bull. Amer. Meteor. Soc.,* **77,** 431–471.

Karsten, R. H., and J. Marshall, 2002: Constructing the residual circulation of the ACC from observations. *J. Phys. Oceanogr.,* **32,** 3315–3327.

Large, W. G., and A. J. G. Nurser, 2001: Ocean surface water mass transformation. *Ocean Circulation and Climate: Observing and Modelling the Global Ocean,* G. Siedler, J. Church, and J. Gould, Eds., International Geophysics Series, Vol. 77, Academic Press, 317–336.

——, G. Danabasoglu, S. C. Doney, and J. C. McWilliams, 1997: Sensitivity to surface forcing and boundary layer mixing in a global ocean model: Annual-mean climatology. *J. Phys. Oceanogr.,* **27,** 2418–2447.

Lee, M.-M., and R. G. Williams, 2000: The role of eddies in the isopycnic transfer of nutrients and their impact on biological production. *J. Mar. Res.,* **58,** 895–917.

——, and A. Coward, 2003: Eddy mass transport in an eddy-permitting global ocean model. *Ocean Modell.,* **5,** 249–266.

Marshall, J., E. Shuckbourgh, H. Jones, and C. Hill, 2006: Estimates and implications of surface eddy diffusivity in the Southern Ocean derived from tracer transport. *J. Phys. Oceanogr.,* **36,** 1806–1821.

McDougall, T. J., and P. C. McIntosh, 2001: The temporal-residual-mean velocity. Part II: Isopycnal interpretation and the tracer and momentum equations. *J. Phys. Oceanogr.,* **31,** 1222–1246.

McIntosh, P. C., and T. J. McDougall, 1996: Isopycnal averaging and the residual mean circulation. *J. Phys. Oceanogr.,* **26,** 1655–1660.

Nowlin, W. D., and J. M. Klinck, 1986: The physics of the Antarctic Circumpolar Current. *Rev. Geophys.,* **24,** 469–491.

Nurser, A. J. G., and M.-M. Lee, 2004a: Isopycnal averaging at constant height. Part I: The exact formulation and a case study. *J. Phys. Oceanogr.,* **34,** 2721–2739.

——, and ——, 2004b: Isopycnal averaging at constant height. Part II: Relating to residual streamfunction. *J. Phys. Oceanogr.,* **34,** 2740–2755.

Olbers, D., and V. O. Ivchenko, 2001: On the meridional circulation and balance of momentum in the Southern Ocean of POP. *Ocean Dyn.,* **52,** 79–93.

Orsi, A. H., T. Whitworth III, and W. D. Nowling Jr., 1995: On the meridional extent and fonts of the Antarctic Circumpolar Current. *Deep-Sea Res.,* **42,** 641–673.

Pacanowski, R. C., 1995: MOM 2 documentation, user's guide and bibreference manual. Geophysical Fluid Dynamics Laboratory/NOAA Ocean Group Tech. Rep. 3, 232 pp.

Phillips, H. E., and S. R. Rintoul, 2000: Eddy variability and energetics from direct current measurements in the Antarctic Circumpolar Current south of Australia. *J. Phys. Oceanogr.,* **30,** 3050–3076.

Sandwell, D. T., and W. H. F. Smith, 1995: Marine gravity from satellite altimetry. The Geological Data Center, Scripps Institution of Oceanography, digital media, version 7.2.

Speer, K., S. R. Rintoul, and B. Sloyan, 2000: The diabatic Deacon cell. *J. Phys. Oceanogr.,* **30,** 3212–3222.

Spencer, R. W., 1993: Global oceanic precipitation from the MSU during 1979–91 and comparisons to other climatologies. *J. Climate,* **6,** 1301–1326.

Stammer, D., 1998: On the eddy mixing and mean flow properties. *J. Phys. Oceanogr.,* **28,** 727–739.

Treguier, A. M., 1999: Evaluating eddy mixing coefficients from eddy-resolving ocean models: A case study. *J. Mar. Res.,* **57,** 89–108.

Webb, D. J., B. A. de Cuevas, and A. C. Coward, 1998: The first main run of the OCCAM global ocean model. Southampton Oceanography Centre Internal Rep. 34, 50 pp. [Available online at http://www.soc.soton.ac.uk/JRD/OCCAM.]

Wijffels, S. E., 2001: Ocean transport of fresh water. *Ocean Circulation and Climate: Observing and Modelling the Global Ocean,* G. Siedler, J. Church, and J. Gould, Eds., International Geophysics Series, Vol. 77, Academic Press, 475–488.

Wunsch, C., 1999: Where do ocean eddy heat fluxes matter? *J. Geophys. Res.,* **104** (C6), 13 235–13 249.

Xie, P., and P. A. Arkin, 1996: Analyses of global monthly precipitation using gauge observations, satellite estimates, and numerical model predictions. *J. Climate,* **9,** 840–858.